A Gasket-Free Electromagnetic Shielding Structure for 2.4-GHz and 5-GHz Bands Using Cascaded Dual-Behavior SIW Resonators

Satoshi Yoneda, Yasuhiro Shiraki, Yuichi Sasaki, and Chiharu Miyazaki

***Abstract*—Various types of electromagnetic shielding structures for specific frequency band have been reported in recent years. A gasket-free electromagnetic shielding structure using folded quarter-wavelength substrate integrated waveguide (FQ-SIW) resonators for 2.4-GHz band is one of them. In the structure, SIW resonators of different resonant frequencies in 2.4-GHz band are cascaded and positioned on inner walls of a gap. The structure is almost free of deterioration since contact-type gaskets are not used. In this paper, a gasket-free electromagnetic shielding structure for 2.4-GHz and 5-GHz bands using cascaded dual-behavior (DB) SIW resonators is proposed and evaluated. A DB-SIW resonator consists of two FQ-SIW resonators sharing one coupling slot and has two almost-independent resonant frequencies in the two bands. The design results showed attenuation characteristics at the two bands, and the configuration was miniaturized by 4% compared with conventional cascaded FQ-SIW resonators. Shielding effectiveness (SE) was also evaluated, and the measured results showed more than 20-dB improvement of SE near the two bands, though frequency shifts were observed.**

***Index Terms*—2.4-GHz band, 5-GHz band, electromagnetic analysis, gasket-free electromagnetic shielding structure, shielding effectiveness (SE), substrate integrated waveguide (SIW) resonator, wireless local area network (WLAN).**

I. Introduction

As WIRELESS local area network (WLAN) devices using 2.4-GHz and 5-GHz bands have been developed and widely spread in recent years, the risks of radio-wave interferences and information leakage have sometimes become problematic. A shielded enclosure is a common and conventional solution, which basically consists of metal walls and shielded doors using contact-type conductive gaskets. However, communication devices using other frequency bands such as cell phones are not available inside, since shielding effectiveness (SE) of the shielded enclosure is continuous in frequency. To realize both SE at WLAN bands and usage of cell phones, a shielded room having frequency selectivity is required. For this requirement, various types of shielding structures have been developed and reported.

For walls and windows of the shielded room, frequency selective surface (FSS) is a standard solution [1]–[9]. FSS basically consists of planar periodic conductive patterns fabricated on a dielectric substrate, and mainly works as a kind of a band stop filter at resonant frequencies of the elements. The FSS is usually designed for decreasing electromagnetic wave whose direction of propagation is almost perpendicular to the surfaces of the walls or the windows. For examples, square-loop periodic elements are used in [1] to obtain SE at 2.4-GHz band, two different-sized "four-legged loaded" elements are used in [2] to obtain narrower bandwidth, full and split ring elements with varactor diodes and surface mount resistors are used in [3] to obtain reconfigurable SE at 2.4-GHz band, two-layered loop and square elements are used in [4] to obtain wide-band SE at 7.5–16.2 GHz, and convoluted square loop elements with six meander peaks on each arm are used on opaque walls in [5] to obtain narrow SE within 1.5–2.5 GHz. Moreover, a combination of rings, loops, and slot elements are used in [6] to obtain either a reject or passband single-layer filter at 2.4 and 5.2 GHz for Wi-Fi applications, five resonant elements are used in [7] to obtain SE at 2.4, 3.5, 4.5, and 5.5 GHz for the security purpose in mobile communication, two-layered conductive and resistive FSSs are used in [8] to obtain low-profile configuration and SE at 5 GHz, and periodic double ring strip FSSs are used in [9] to obtain SE at 2.45- and 5.4-GHz bands.

A shielded room usually has a shielded door, where a gap exists between the door and the door frame. Conductive gaskets are generally applied for realizing SE at the gap. The conductive gaskets are usually contact-type that electrically connect the shielded door and the door frame when the door is closed. Though relatively high SE can be realized by applying them, their SE is continuous in frequency and they are not suitable for realizing SE at specific frequency bands. Since high contact pressure is required to obtain high SE, an ordinary simple door configuration is usually not applicable. Furthermore, through the opening and closing operations of the door, aged deterioration mainly caused by metal fatigue is inevitable, and periodic maintenance is necessary. Aged deterioration caused by corrosive environments is reported in [10], and the reliability of a conductive gasket is assessed by using a TEM cell in [11] or

Manuscript received September 13, 2018; revised January 9, 2019; accepted February 15, 2019. Date of publication April 9, 2019; date of current version April 14, 2020. *(Corresponding author: Satoshi Yoneda.)*

The authors are with the Mitsubishi Electric Corporation Information Technology R&D Center, Kamakura 247-8501, Japan (e-mail: yoneda-satoshi@mext.go.jp; Shiraki.Yasuhiro@db.MitsubishiElectric.co.jp; Sasaki.Yuichi@dw.MitsubishiElectric.co.jp; Miyazaki.Chiharu@ah.MitsubishiElectric.co.jp).

Color versions of one or more of the figures in this paper are available online at http://ieeexplore.ieee.org.

Digital Object Identifier 10.1109/TEMC.2019.2902605

TABLE I
COMPARISON OF THE RFERRED SHIELDING STRUCTURES

Shielding structures [ref]	FSS [1-9]	Conductive Gasket [10-13]	Magnetic absorber [14]	Cascaded SIW resonators [15, 16] (and this work)
Applicable area	Walls	Gap between door and door frame	Gap between door and door frame	Gap between door and door frame
Applicable frequency range	Several GHz to several-tens GHz	All ranges (ideally)	kHz to several GHz	Several GHz to several-tens GHz
Frequency selectivity	Applicable	N/A	N/A	Applicable

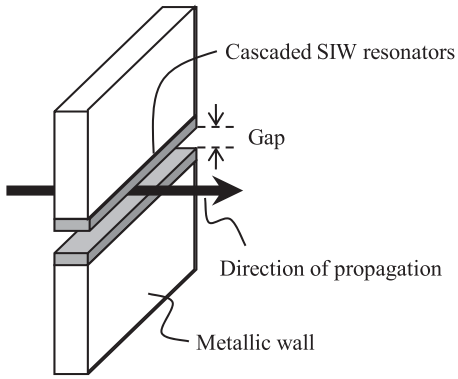

Fig. 1. Simplified configuration of the gasket-free shielding structure. Cascaded SIW resonators are placed on the inner walls of the gap.

a stripline setup in [12]. Several types of conductive gaskets in environmentally worst-cases are modeled and their SE are estimated and compared with simulated results in [13].

Some gasket-free shielding structures applicable for the gap of the shielded door and the door frame are reported [14]–[16]. Since the structures are not contact-type, the high contact pressure is not needed even when the door is closed. Therefore, an ordinary simple door configuration is applicable, and moreover, they are almost free of the aged deterioration. In [14], several kinds of magnetic materials, called magnetic absorbers, are positioned on the inner walls of the gap and measured results showed 15-dB improvement of SE in a wide frequency band from 100 MHz to 2.5 GHz. As other gasket-free shielding structure for the gap, ones using substrate integrated waveguide (SIW) resonators are reported [15], [16]. An SIW resonator is a kind of a resonant cavity embedded in a dielectric substrate by conductive patterns and via holes [17] and has been widely applied for high-frequency microwave applications. In the structures, SIW resonators are arranged in a cascaded configuration and placed on inner walls of a gap. The structure works as a kind of a band stop filter at the resonance frequencies of the cascaded SIW resonators. A double-sided substrate is applied for SIW resonators used in [15] to obtain SE at 12–16 GHz, and a multi-layered substrate is applied for folded quarter-wavelength (FQ) SIW resonators used in [16] to obtain SE at 2.4-GHz band with practical size. Basically, the configurations reported in [15] and [16] can obtain SE at one frequency band. Therefore, additional cascaded SIW or FQ-SIW resonators are required to obtain SE at multi-bands, 2.4-GHz and 5-GHz bands of WLAN for example.

The shielding structures referred above are compared in Table I, showing their applicable areas and frequency ranges, as well as frequency selectivity. Some other shielding techniques are reported in [18]–[20]. Magnetic materials are used to mitigate the magnetic field leaked from the joint parts of a shielded enclosure at several kHz up to several hundreds of kHz, and showed 20-dB improvement of SE [18]. Alternatives to conductive gaskets are studied in [19], and experimental results showed that grounding points or lossy materials can be used instead of conductive gaskets below 1 GHz, if no more than 30 dB of SE is needed. A door-less access passage to a shielded enclosure is studied in [20], where some design rules and limitations of the passage are presented.

In this paper, a gasket-free shielding structure for 2.4-GHz and 5-GHz bands using cascaded dual-behavior (DB) SIW resonators is proposed and evaluated. A DB-SIW resonator consists of two FQ-SIW resonators sharing one coupling slot and has two almost-independent resonant frequencies. A prototype structure for 2.4-GHz and 5-GHz bands was designed by EM-analysis using an eight-layered FR4 substrate. The design results showed attenuation characteristics at 2.4-GHz and 5-GHz bands, and the configuration had 4% miniaturized size compared with cascaded FQ-SIW resonators having the same resonant frequencies. Two fabricated substrates were placed on the inner walls of a gap. Two antennas connected to a two-port network analyzer were placed to face each other across the gap, and SE of the structure were evaluated by measuring the transmission coefficients between the antennas with and without the substrates. The measured results showed more than 20-dB improvement of SE near the two bands, though some frequency shifts were observed. From the EM-analysis results after the measurements, it was cleared that the main reason for the frequency shifts was likely to be the manufacturing error in the size of the via holes.

II. CONFIGURATION

Fig. 1 shows a simplified configuration of the gasket-free shielding structure. Cascaded SIW resonators are embedded in substrates placed on the upper and lower inner walls of the gap. When an electromagnetic wave propagates through the gap, each SIW resonator resonates at its own resonant frequency, and propagation is suppressed at the frequency. As a result, the structure works as a kind of a band stop filter at the resonant frequencies, thus SE at the specific frequency bands can be realized [15]. Fig. 2 shows a cascaded configuration of conventional SIW resonators. The surfaces of the substrate are covered with conductive patterns except for coupling slits, and the coupling slits and via-hole arrays are placed alternately along the direction of propagation. At each SIW resonator, the coupling slit is positioned at the center, and the distance between the via-hole

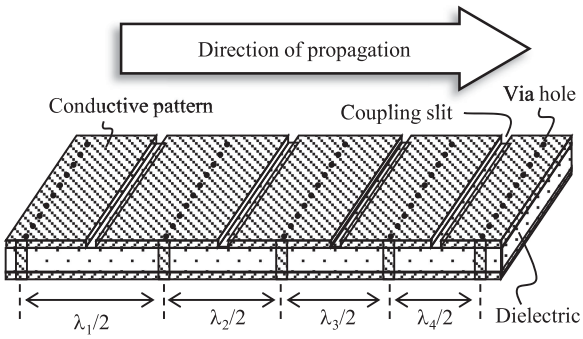

Fig. 2. Cascaded configuration of conventional SIW resonators. The distance between the via-hole arrays at each SIW resonator is half-wavelength at its own resonant frequency.

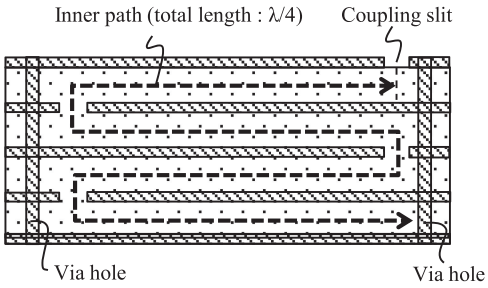

Fig. 3. Cross-sectional view of an FQ-SIW resonator. The inner path is folded in a multi-layered configuration, and its total length is quarter-wavelength at the resonant frequency.

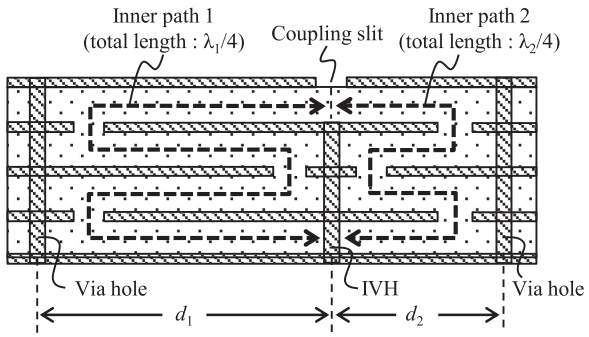

Fig. 4. Cross sectional view of a DB-SIW resonator. The resonator has two independent inner paths, and two almost-independent resonant frequencies.

arrays is half wavelength at its resonant frequency. In the case of applying this resonator at 2.4 GHz using an ordinary FR4 substrate, the half-wavelength becomes almost 30 mm, hence it is difficult to realize the cascaded configuration of the conventional SIW resonators with practical size. An FQ-SIW resonator is one of the solutions for this problem. Fig. 3 shows a cross-sectional view of an FQ-SIW resonator, where the inner path is folded in a multi-layered configuration and the total length of the path is a quarter wavelength at the resonant frequency. Since the distance between the via-hole arrays of an FQ-SIW resonator is much smaller than that of a conventional SIW resonator, it becomes possible to realize the cascaded configuration of FQ-SIW resonators for 2.4-GHz band with practical size [16].

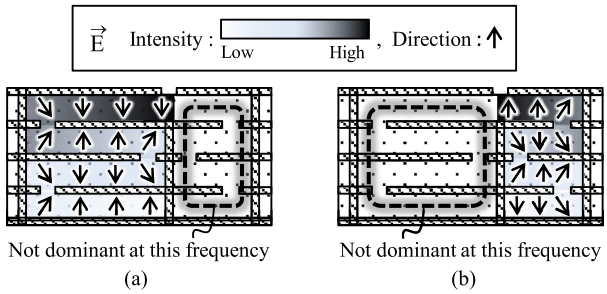

Fig. 5. E-fields at two resonant frequencies. Total length of the inner path 1 is quarter wavelength at the resonant frequency f_1, while that of the inner path 2 is quarter wavelength at the resonant frequency f_2. (a) At the resonant frequency f_1. (b) At the resonant frequency f_2.

Fig. 4 shows a cross-sectional view of a DB-SIW resonator that consists of two FQ-SIW resonators sharing one coupling slit. Note that an interstitial via hole (IVH) is positioned underneath the coupling slit. As shown in the figure, a DB-SIW resonator has two independent inner paths, and hence, has two almost-independent resonant frequencies as well. Fig. 5 shows E-fields at the two resonant frequencies. At a resonant frequency f_1, when the total length of the inner path 1 is equal to a quarter wavelength, the intensity of the E-field is the highest at the coupling slit and the lowest at the end of the inner path 1 as shown in Fig. 5(a). At another resonant frequency f_2, when the total length of the inner path 2 is equal to a quarter wavelength, the intensity of the E-field is the highest at the coupling slit as well and the lowest at the end of the inner path 2 as shown in Fig. 5(b).

A configuration of cascaded two FQ-SIW resonators has also two independent inner paths. However, compared with the cascaded two FQ-SIW resonators, miniaturization can be expected in a DB-SIW resonator since one coupling slit is removed by integrating two coupling slits into one.

III. Design Process

To design cascaded DB-SIW resonators for 2.4-GHz band (2.35–2.55 GHz) and 5-GHz band (5.10–5.80 GHz), a design process for a single DB-SIW resonator must be cleared first. Resonant frequencies of the DB-SIW resonator, f_1 and f_2, can be roughly estimated by

$$d_i = \frac{1}{N-1}\left(\frac{c}{4f_i\sqrt{\varepsilon_{\mathrm{r}}}}\right) \ (i = 1, 2) \tag{1}$$

where d_1 and d_2 are the distance between a via hole and an IVH of each inner path, N is the number of conductor layers in the multi-layered configuration, ε_r is the relative dielectric constant of the substrate, and c is the speed of light. Since this equation is just for a rough estimation, the more accurate equation is preferable for the design process. To improve the accuracy, an EM-analysis and a numerical approximation are applicable.

Fig. 6 shows the EM-analysis model of a 1st-order DB-SIW resonator. A gap is modeled by a thin vacuum box of 3-mm height and 0.8-mm width, and note that the sidewalls are defined as magnetic walls which work as symmetric boundaries. Eight-layered FR4 substrates [ε_r : 4.3, $\tan\delta$: 0.016, thickness:

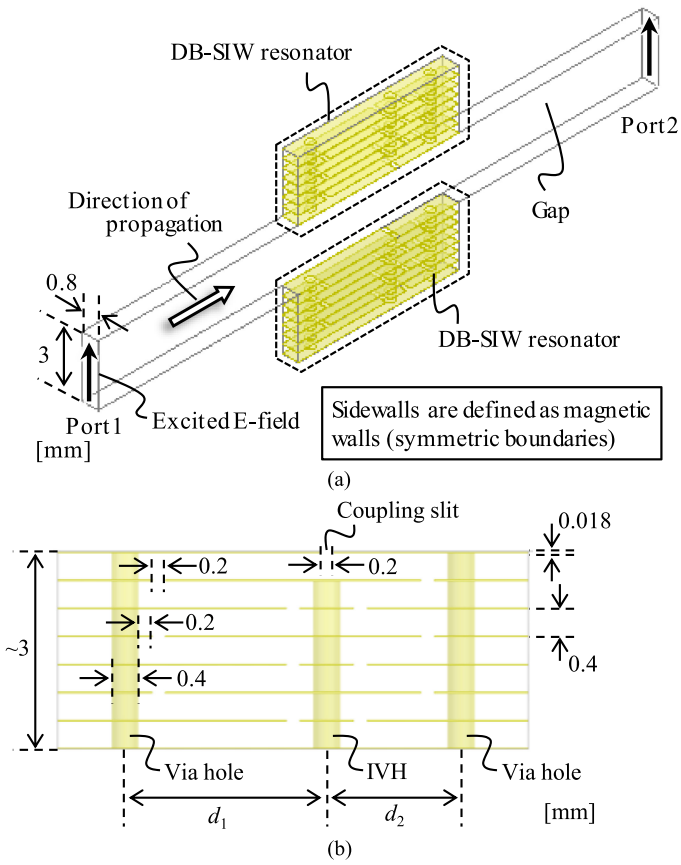

Fig. 6. EM-analysis model of a 1st-order DB-SIW resonators. DB-SIW resonators are placed on the upper and lower inner wall of the gap. (a) Perspective view. (b) Cross-sectional view.

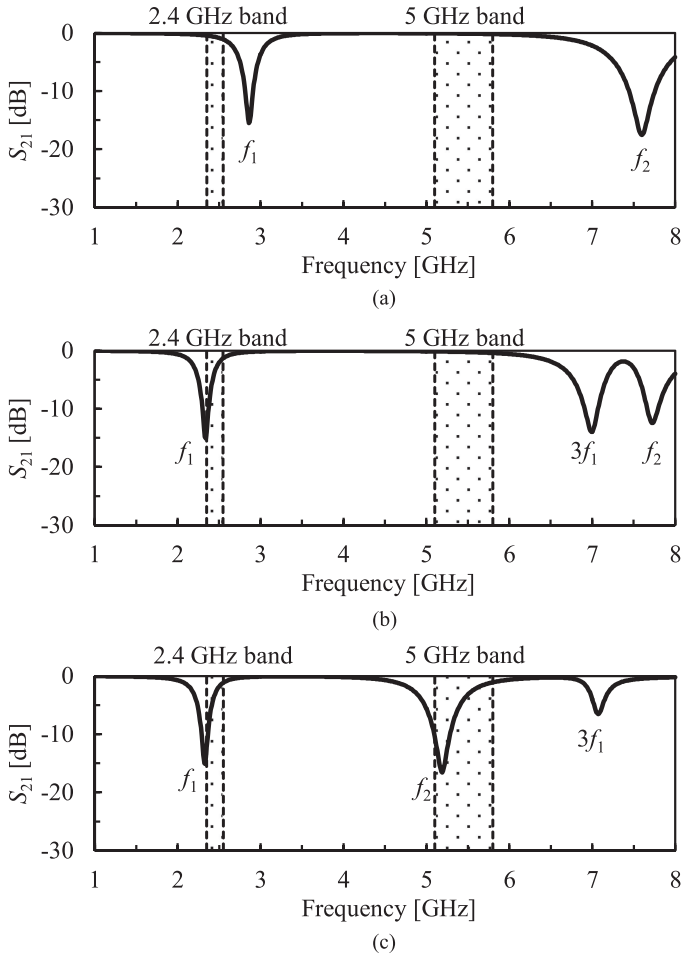

Fig. 7. EM-analysis results of S_{21}. $f_1 = 2.35$ GHz and $f_2 = 5.1$ GHz were almost obtained with $d_1 = 2.6$ mm and $d_2 = 1.4$ mm. (a) $d_1 = 2.2$ mm, $d_2 = 1.0$ mm (initial values. (b) $d_1 = 2.6$ mm, $d_2 = 1.0$ mm). (c) $d_1 = 2.6$ mm, $d_2 = 1.4$ mm.

0.4 mm (dielectric layers), 18 μm (conductive layers)] are placed on the upper and lower inner walls of the gap, and one DB-SIW resonator is embedded in each substrate. The diameters of via holes and IVHs are 0.4 mm, their pitch is 0.8 mm, and the shortest distance from the hole-edge to the pattern-edge is 0.2 mm. The distances between the via-holes and the IVH along the direction of propagation are defined as d_1 and d_2, and width of both the coupling slit and slits of the inner-conductive layers are 0.2 mm. Port 1 and Port 2 are defined at the edges of the gap, and the electromagnetic wave propagating through the gap is modeled by a vertically excited E-field at Port 1. In the EM-analysis results of this model, S_{21} forms attenuation poles at resonant frequencies of the DB-SIW resonators.

The initial values of d_1 and d_2 can be roughly estimated from (1). For examples, by substituting $f_1 = 2.35$ GHz and $f_2 = 5.10$ GHz into (1), $d_1 = 2.2$ mm and $d_2 = 1.0$ mm were obtained. From this result, $d_1 = 2.2$ mm and $d_2 = 1.0$ mm were chosen as initial values. Fig. 7(a) shows the EM-analysis result of S_{21} with these initial values, indicating that d_1 and d_2 should be increased since f_1 and f_2 are higher than expected. From the EM-analyses with increased d_1 from 2.2 mm, it was clear that f_1 became almost 2.35 GHz when $d_1 = 2.6$ mm. Fig. 7(b) shows the EM-analysis result of S_{21} with $d_1 = 2.6$ mm and $d_2 = 1.0$ mm, showing $f_1 = 2.35$ GHz. Note that the attenuation pole at 7 GHz can be comprehensible as a harmonic response of f_1. In the same way, from the EM-analyses with increased d_2 from 1.0 mm whereas d_1 is fixed to 2.6 mm, it was cleared that f_2 becomes almost 5.1 GHz when $d_2 = 1.4$ mm. Fig. 7(c) shows the EM-analysis result of S_{21} with $d_1 = 2.6$ mm and $d_2 = 1.4$ mm, showing that both $f_1 = 2.35$ GHz and $f_2 = 5.1$ GHz are almost obtained.

Before deriving the design equations, the independency of f_1 from d_2 and f_2 from d_1 should be confirmed. Fig. 8 shows an extracted f_1 and f_2 from the EM-analysis results with d_1 varied from 2.0 mm to 3.0 mm and d_2 varied from 1.0 mm to 2.0 mm. Since f_1 is well stable against d_2 and f_2 is also well stable against d_1 in the figures, the independency was confirmed within 2.0 mm $\leq d_1 \leq$ 3.0 mm and 1.0 mm $\leq d_2 \leq$ 2.0 mm. From this result, $d_1(f_1)$ can be derived as an approximated equation of the EM-analysis results with d_1 varied from 2.0 mm to 3.0 mm and d_2 fixed to 1.4 mm. In the same way, $d_2(f_2)$ can be derived as an approximated equation of the EM-analysis results with d_2 varied from 1.0 mm to 2.0 mm and d_1 fixed to 2.6 mm.

Fig. 9 shows the EM-analysis results and the approximated equations of $d_1(f_1)$ and $d_2(f_2)$. In the approximating process, a

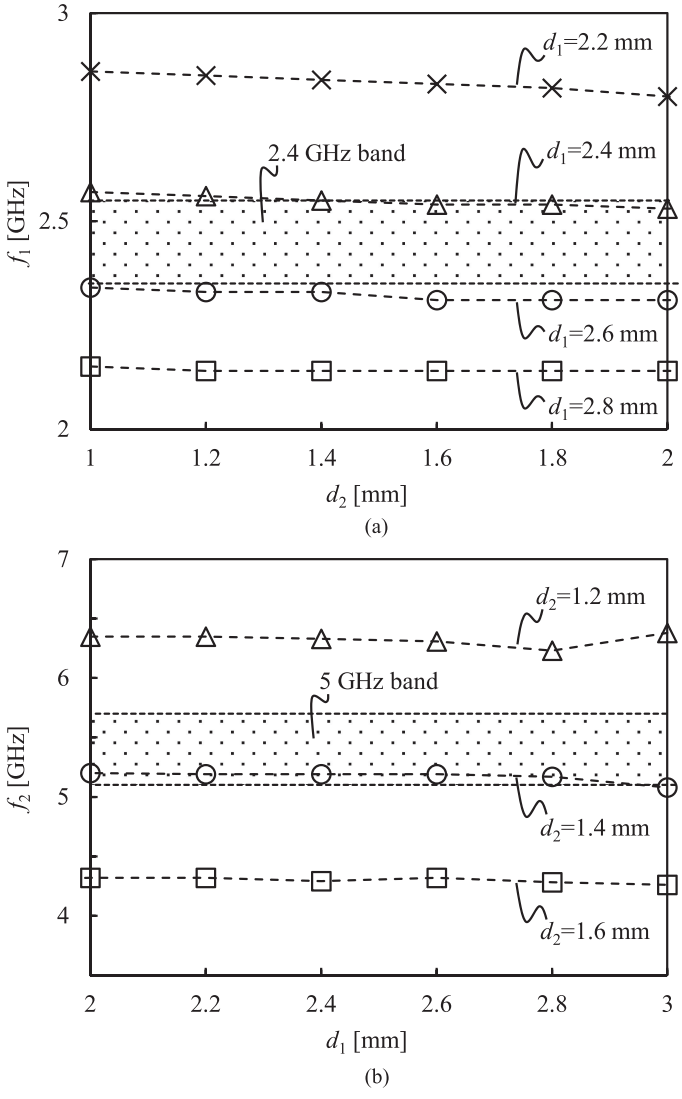

Fig. 8. Extracted f_1 and f_2 from EM-analysis results with d_1 varied from 2.0 mm to 3.0 mm and d_2 varied from 1.0 mm to 2.0 mm. Both f_1 and f_2 are well stable in the figures. (a) Extracted f_1. (b) Extracted f_2.

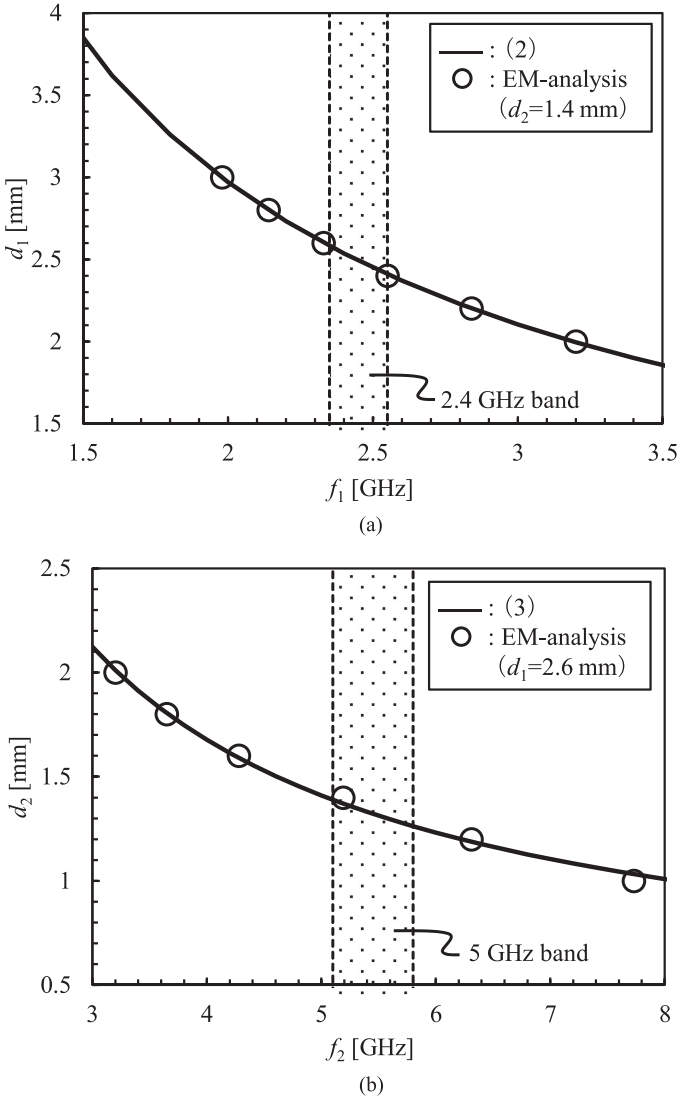

Fig. 9. EM-analysis results and approximated equations of $d_1(f_1)$ and $d_2(f_2)$. The approximated equations, (2) and (3), correlate well with the EM-analysis results. (a) $d_1(f_1)$. (b) $d_2(f_2)$.

1st-order linear equation of $1/f_i$ $(i = 1, 2)$ was applied for the equations from the rough estimation (1), and the least square method was applied. The obtained equations were

$$d_1(f_1) = 5.20\frac{1}{f_1\,[\mathrm{GHz}]} + 0.37 \quad [\mathrm{mm}] \tag{2}$$

$$d_2(f_2) = 5.35\frac{1}{f_2\,[\mathrm{GHz}]} + 0.34 \quad [\mathrm{mm}]. \tag{3}$$

The approximated equations correlate well with the EM-analysis results, hence, the 1st-order expression of $1/f_i$ $(i = 1, 2)$ would be sufficient for the design equation in this case.

A cascaded configuration of DB-SIW resonators can be designed by cascading DB-SIW resonators having resonant frequencies in each shield band. Before designing the individual DB-SIW resonator, the order number of the cascaded configuration must be determined. The permitted length of the configuration along the direction of propagation was 50 mm this time. The DB-SIW resonator with $f_1 = 2.35$ GHz and $f_2 = 5.10$ GHz has the largest d_1 and d_2, and $d_1 = 2.58$ mm and $d_2 = 1.39$ mm can be obtained from (2) and (3) for these frequencies.

The size of the largest DB-SIW resonator along the direction of propagation is then 3.97 mm, which is the sum of d_1 and d_2. By comparing this size with the permitted length of 50 mm, the order number of the cascaded configuration was estimated to be 12. By the 12th-order cascaded configuration of DB-SIW resonators, 12 independent resonant frequencies within both 2.4-GHz and 5-GHz bands can be designed.

Fig. 10 shows the EM-analysis model of the 12th-order cascaded DB-SIW resonators. Twelve DB-SIW resonators (#1–#12) are cascaded along the direction of propagation and placed on the upper and lower inner walls of the gap. Note that the side walls are defined as magnetic walls that work as symmetric boundaries same as the model shown in Fig. 6(a).

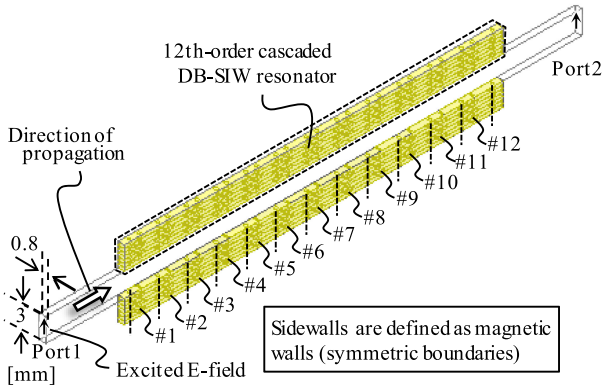

Fig. 10. EM-analysis model of the 12th-order cascaded DB-SIW resonators. 12 DB-SIW resonators are cascaded along the direction of propagation.

TABLE II
f_1, f_2, d_1, AND d_2 OF THE DESIGNED DB-SIW RESONATORS

	f_1 [GHz]	f_2 [GHz]	d_1 [mm]	d_2 [mm]
#1	2.35	5.10	2.58	1.39
#2	2.37	5.16	2.57	1.38
#3	2.39	5.23	2.55	1.36
#4	2.40	5.29	2.53	1.35
#5	2.42	5.35	2.52	1.34
#6	2.44	5.42	2.50	1.33
#7	2.46	5.48	2.48	1.32
#8	2.48	5.55	2.47	1.30
#9	2.50	5.61	2.45	1.29
#10	2.51	5.67	2.44	1.28
#11	2.53	5.74	2.42	1.27
#12	2.55	5.80	2.41	1.26

The 12 resonant frequencies within each shield band were selected to have equal frequency intervals in each shield band. Table II shows f_1, f_2, d_1, and d_2 of the DB-SIW resonators, where d_1 and d_2 were obtained from (2) and (3). For a comparison, 24th-order cascaded FQ-SIW resonators having the same 24 resonant frequencies on Table II were also designed by the design process in [16] using the same substrate. Fig. 11 shows the EM-analysis results of S_{21} of the two designed configurations, demonstrating that attenuation characteristics at 2.4 GHz and 5 GHz bands are achieved by both configurations and that the two results are comparable. The total length along the direction of propagation were 45.79 mm for the 12th-order cascaded DB-SIW resonators, and 47.82 mm for the 24th-order cascaded FQ-SIW resonators. These results indicate that the cascaded DB-SIW resonators can realize attenuation characteristics comparable to that of the cascaded FQ-SIW resonators with a configuration 4%-miniaturized along the direction of propagation.

IV. EXPERIMENTAL RESULTS

The designed cascaded DB-SIW resonators were fabricated and SE was evaluated. Fig. 12 shows a measurement system for

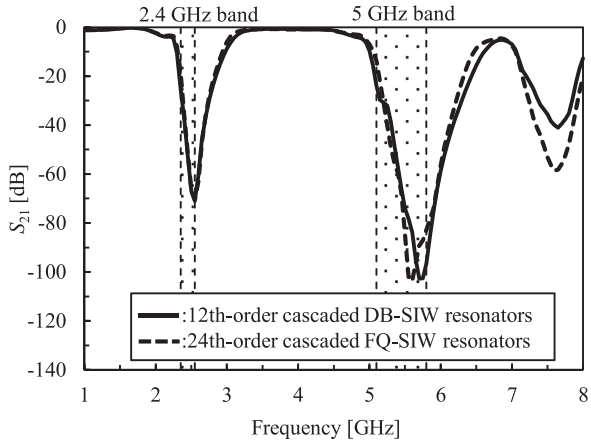

Fig. 11. EM-analysis results of S_{21} of the two designed configurations. Attenuation characteristics at 2.4-GHz and 5-GHz bands are achieved by both configurations and two results are comparable.

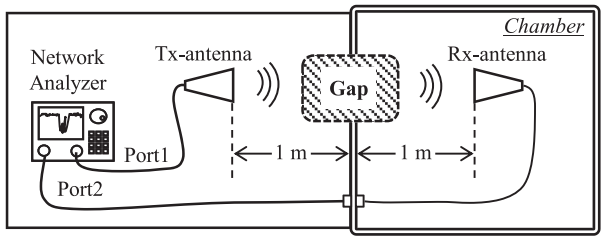

Fig. 12. Measurement system for evaluating SE. The gap is located on the wall of a shielded chamber.

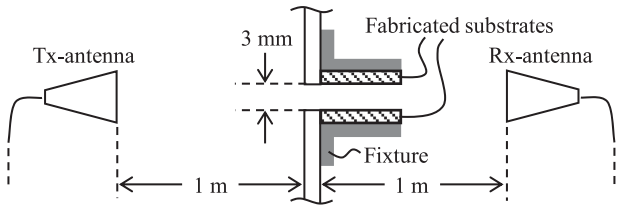

Fig. 13. Cross-sectional view of the gap. Two fabricated substrates are affixed to L-shaped fixtures fixed on the wall of the chamber.

evaluating SE. Tx and Rx antennas are positioned to face each other across the gap of 200 mm × 3 mm aperture size located on the wall of a shielded chamber. The Tx antenna is placed outside the chamber at 1 m away from the wall and connected to Port 1 of a network analyzer. On the other hand, the Rx antenna is placed inside the chamber at 1 m away from the wall and connected to Port 2 of the network analyzer. With this measurement system, SE can be evaluated by measured results of the transmission coefficient, S_{21}. Fig. 13 shows a cross-sectional view of the gap, and Fig. 14 shows the gap seen from the Tx- and the Rx-antenna sides. Two fabricated substrates are affixed to L-shaped fixtures of the copper plate by conductive double-sided tape, and the fixtures are fixed on the wall of the chamber. At the space between the Tx antenna and the gap, the electromagnetic wave propagates with TEM mode. At the aperture of the gap, the electric field between two long sides of the aperture is excited by

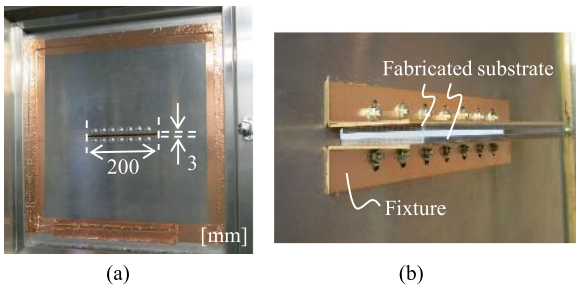

Fig. 14. Gap seen from the Tx and the Rx antenna sides. Aperture size of the gap is 200 mm × 3 mm. (a) Tx-antenna side. (b) Rx-antenna side.

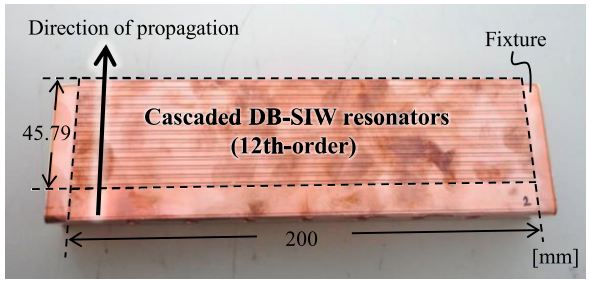

Fig. 15. Fabricated substrate of cascaded DB-SIW resonators. 12 DB-SIW resonators are cascaded along the direction of propagation in 45.79 mm.

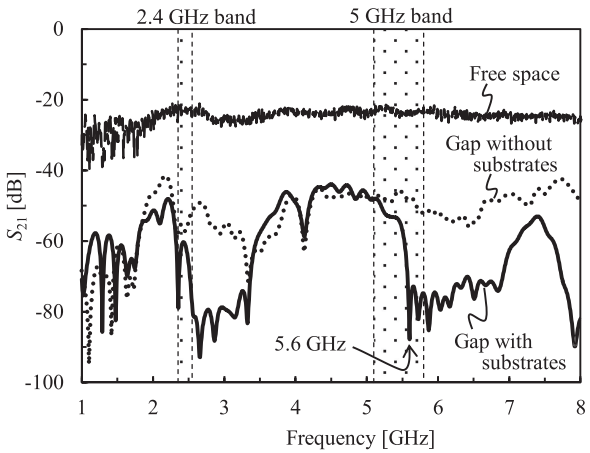

Fig. 16. Measured result of S_{21} of free space, the gap without the substrates, and the gap with the substrates.

the electromagnetic wave. Therefore, the dominant mode of the electromagnetic wave inside the gap is TE mode. At the space between the gap and the Rx antenna, the electromagnetic wave propagates with TEM mode again. Fig. 15 shows the fabricated eight-layered FR4 substrates whose dielectric constant and other parameters are the same as those used in the EM-analyses in the design process.

Fig. 16 shows the results of S_{21} measured in free space, and through the gap with or without the substrates. The measured frequency range is 1–8 GHz with the frequency interval of 5.6 MHz. SE can be evaluated by defining the measured S_{21} of free space as a reference. Fig. 17 shows SE of the gap with and without the substrates. The measured result showed more

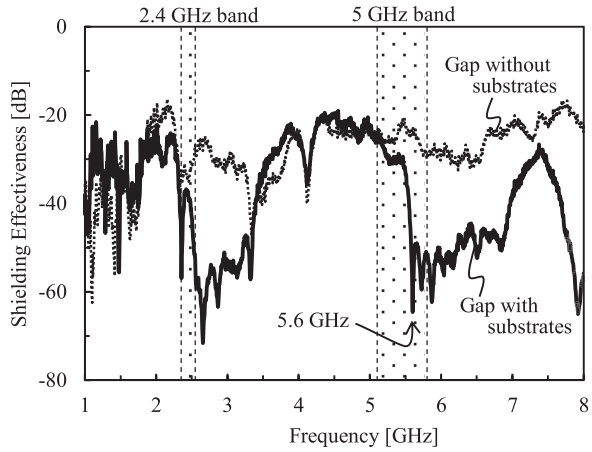

Fig. 17. Measured result of SE of the gap without the substrates, and the gap with the substrates. The measured result of S_{21} of free space in Fig. 15 is defined as 0-dB reference.

TABLE III
FREQUENCY SHIFTS CALCULATED FROM THE EM-ANALYSIS RESULTS

	Items	Design value	Manufacturing error	Frequency shift
(a)	Dielectric constant	4.3	- 0.1 + 0.1	+ 1.0% - 1.1%
(b)	Width of the slits	0.2 mm	- 0.03 mm + 0.03 mm	- 4.6% + 4.4%
(c)	Diameter of the via holes	0.4 mm	- 0.1 mm + 0.1 mm	- 9.5% + 10.1%
	Measured Result	-	-	+ 9.8 %

than 20 dB improvement of SE near the two bands, though some frequency shift was observed.

A cause of the frequency shift must become clear for the practical use of this configuration, and the cause can be extrapolated by comparing the EM-analysis and the measured results. The lowest resonant frequency of the cascaded DB-SIW resonators in 5-GHz band was designed to be 5.1 GHz as shown in Table II. In the measured results, however, the lowest resonant frequency in 5-GHz band which is indicated by the lowest attenuation pole in 5-GHz band was 5.6 GHz. Thus, from these two frequencies, the frequency shift in the measured results can be estimated as +9.8%. This frequency shift could have been caused by manufacturing errors: (a) dielectric constant (4.3 ± 0.1), (b) width of the slits (0.2 ± 0.03 mm), and (c) diameter of via holes (0.4 ± 0.1 mm), for examples. Potential frequency shifts due to these manufacturing errors can be estimated by EM-analysis. Fig. 18 shows the EM-analysis results of the 1st-order DB-SIW resonators considering each of these manufacturing errors. The DB-SIW resonator indicated as #1 in Table II is used in the model ($d_1 = 2.58$ mm and $d_2 = 1.39$ mm). Table III shows the frequency shift calculated from the resonant frequencies in 5-GHz band of the EM-analysis results. Compared with the

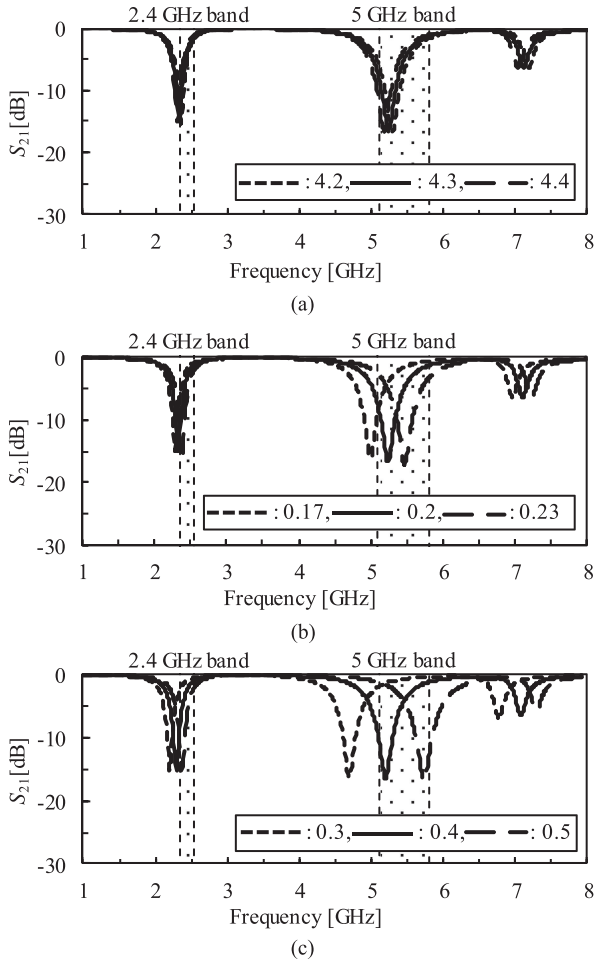

Fig. 18. EM-analysis results of the 1st-order DB-SIW resonators considering three manufacturing errors using the resonators indicated as #1 in Table I. (a) Dielectric constant (4.3 ± 0.1). (b) Width of the slits $(0.2 \pm 0.03$ mm). (c) Diameter of via holes $(0.4 \pm 0.1$ mm).

frequency shift of the measured results, it can be inferred that the main reason for the frequency shift was the manufacturing error of the diameter of via holes.

V. Conclusion

A gasket-free electromagnetic shielding structure for 2.4-GHz and 5-GHz bands using cascaded DB-SIW resonators is proposed and evaluated in this paper. A DB-SIW resonator consists of two FQ-SIW resonators sharing one coupling slot, and has two almost-independent resonant frequencies. In the structure, DB-SIW resonators having resonant frequencies in both 2.4-GHz and 5-GHz bands are cascaded along the direction of propagation and placed on the inner walls of a gap. The structure works as a kind of a band stop filter at the resonance frequencies of the cascaded DB-SIW resonators. For its non-contact configuration, it has mainly two advantages: an ordinary simple door configuration is applicable and being almost free of aged deterioration.

A configuration for 2.4-GHz and 5-GHz bands was designed with an eight-layered FR4 substrate according to the design process based on an EM-analysis and a numerical approximation. As a result, 12th-order cascaded DB-SIW resonators was designed with a size of 45.79 mm along the direction of propagation, and the EM-analysis result showed attenuation characteristics at the two bands. Prototype substrates were fabricated and SE of the shielding structure was evaluated. The measured result showed more than 20 dB improvement of SE near the two bands, though some frequency shift was observed. From the EM-analysis results considering some manufacturing errors, it was inferred that the main reason for the frequency shift was the manufacturing error of the diameter of via holes.

References

[1] M. Raspopoulos and S. Stavrou, "Frequency selective buildings through frequency selective surfaces," *IEEE Trans. Antennas Propag.*, vol. 59, no. 8, pp. 2998–3005, Aug. 2011.

[2] M. Kartal, B. Doken, and I. Gungor, "Design for the structural surface material enabling shielding for interference mitigation within the buildings in the unlicensed 2.4GHz ISM band," in *Proc. Gen. Assem. Sci. Symp.*, Istanbul, Turkey, Aug. 2011, pp. 1–4.

[3] B. Sanz-Izquierdo and E. A. Parker, "Dual polarized reconfigurable frequency selective surfaces," *IEEE Trans. Antennas Propag.*, vol. 62, no. 2, pp. 764–771, Feb. 2014.

[4] S. Habib, G. I. Kiani, and M. F. U. Butt, "An efficient UWB FSS for electromagnetic shielding," in *Proc. Int. Conf. Electromagn. Adv. Appl.*, Verona, Italy, Sep. 2017, pp. 1543–1546.

[5] A. A. Dewani, S. G. O'Keefe, D. V. Thiel, and A. Galehdar, "Window RF shielding film using printed FSS," *IEEE Trans. Antennas Propag.*, vol. 66, no. 2, pp. 790–796, Feb. 2018.

[6] D. Ferreira, T. Fernandes, I. Cuiñas, and R. Caldeirinha, "A dual-band single-layer frequency selective surface for Wi-Fi applications," in *Proc. 9th Eur. Conf. Antennas Propag.*, Lisbon, Portugal, Apr. 2015, pp. 1–4.

[7] N. Choudhary, A. Sharma, and S. Yadav, "A novel band stop frequency selective surface for the security of quad band mobile applications," in *Proc. IEEE Appl. Electromagn. Conf.*, Maharashtra, India, Dec. 2017, pp. 1–2.

[8] S. Habib, G. I. Kiani, and M. F. U. Butt, "An efficient FSS absorber for WLAN security," in *Proc. IEEE Int. Symp. Antennas Propag. USNC-URSI Radio Sci. Meet.*, San Diego, CA, USA, Jul. 2017, pp. 689–690.

[9] X. Xiong, W. Hong, Z. Zhao, L. Deng, and S. Li, "WiFi band-stop FSS for increased privacy protection in smart building," in *Proc. IEEE 6th Intern. Symp. Microw., Antenna, Propag., EMC Technol.*, Shanghai, China, Oct. 2015, pp. 826–828.

[10] H. W. Denny and K. R. Shouse, "EMI shielding of conductive gaskets in corrosive environments," in *Proc. IEEE Intern. Symp. Electromagn. Compat.*, Washington, D.C., USA, Aug. 1990, pp. 20–24.

[11] P. Faraji, J. L. Drewniak, D. S. McBain, and D. Pommerenke, "SE measurements with a TEM cell to study gasket reliability," in *Proc. IEEE Intern. Symp. Electromagn. Compat.*, Denver, CO, USA, Aug. 2013, pp. 462–465.

[12] T. Claeys, J. Catrysse, D. Pissoort, and Y. Arien, "Stripline set-up for characterizing the effect of corrosion and ageing on the shielding effectiveness of emi gaskets with improved repeatability," in *Proc. EMC Eur.*, Amsterdam, The Netherlands, Aug. 2018, pp. 725–729.

[13] D. Tsyanenka, Y. Arlou, and E. Sinkevich, "Worst-case model for considering gaskets in calculation of shielding effectiveness of metallic enclosures," in *Proc. EMC Eur.*, Amsterdam, The Netherlands, Aug. 2018, pp. 178–183.

[14] Y. Murata, T. Kanamoto, and F. Murase, "Wideband shield door with a magnetic absorber," *IEEE Trans. Electromagn. Compat.*, vol. 55, no. 3, pp. 526–531, Jun. 2013.

[15] S. Yoneda, Y. Shiraki, Y. Sasaki, N. Oka, and H. Oh-Hashi, "A GHz-band gasket-free electromagnetic shielding structure with built-in cascaded SIW resonators," in *Proc. EMC Eur. 2014*, Gothenburg, Sweden, Sep. 2014, pp. 432–437.

[16] S. Yoneda, Y. Shiraki, Y. Sasaki, N. Oka, and H. Oh-Hashi, "A gasket-free electromagnetic shielding structure for 2.4 GHz band using folded quarter-wavelength SIW resonators," in *Proc. IEEE Int. Symp. Electromagn. Compat.*, Ottawa, ON, Canada, Jul. 2016, pp. 271–276.

[17] D. Deslandes and K. Wu, "Accurate modeling, wave mechanisms, and design considerations of a substrate integrated waveguide," *IEEE Trans. Microw. Theory Techn.*, vol. 54, no. 6, pp. 2516–2526, Jun. 2006.
[18] T. Tsuruta, S. Hirosato, and K. Fujiwara, "High performance shield room for intermediate frequency magnetic fields," in *Proc. EMC Eur.*, Gothenburg, Sweden, Sep. 2014, pp. 1069–1073.
[19] F. Centola, D. J. Pommerenke, X. Kai, and J. L. Drewniak, "Alternatives to gaskets in shielding an enclosure," in *Proc. IEEE Int. Symp. Electromagn. Compat.*, Minneapolis, MN, USA, Aug. 2002, pp. 205–209.
[20] V. Rodriguez, "On the design of door-less access passages to shielded enclosures," in *Proc. Antenna Meas. Techn. Assoc. Symp.*, Atlanta, GA, USA, Oct. 2017, pp. 1–6.

Satoshi Yoneda received the B.S. and M.S. degrees in physics from Tokyo University, Tokyo, Japan, in 2000 and 2002, respectively.

In 2002, he joined the Mitsubishi Electric Corporation, Kamakura, Japan. His current research interests include electromagnetic compatibility (EMC) technologies.

Mr. Yoneda was the recipient of the Best Paper Award of EMC Europe 2014.

Yasuhiro Shiraki received the B.E., M.E., and Ph.D. degrees in electrical engineering from Okayama University, Okayama, Japan, in 1989, 1991, and 2006, respectively.

In 1991, he joined the Mitsubishi Electric Corporation, Amagasaki, Japan, where he is currently a Senior Researcher with the Electromechanical Systems Department, Advanced Technology R&D Center. His research interests include electromagnetic compatibility (EMC) design for power electronics, EMC measurement techniques, and electromagnetic simulation.

Yuichi Sasaki received the B.E. degree in control system engineering from Tokai University, Kanagawa, Japan, in 1991.

In 1991, he joined the Mitsubishi Electric Corporation, Kamakura, Japan. His current research interests include high-speed signal transmission and electromagnetic compatibility (EMC) technologies.

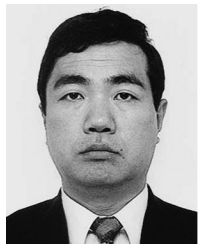

Chiharu Miyazaki received the B.E., M.E., and Ph.D. degrees in electrical engineering from the Musashi Institute of Technology, Tokyo, Japan, in 1987, 1989, and 2006, respectively.

In 1989, he joined the Mitsubishi Electric Corporation, Kamakura, Japan. His current research interests include electromagnetic compatibility technologies.